

Pulse delay of a stimulated Raman process in atomic vapor

Jianmin Li,¹ Zhifei Yu,¹ L. Q. Chen,^{1,2,*} Chun-Hua Yuan,^{1,2,†} Guzhi Bao,¹ Yuan Wu,¹ and Weiping Zhang^{2,3}

¹*Department of Physics, East China Normal University, Shanghai 200062, People's Republic of China*

²*Collaborative Innovation Center of Extreme Optics, Shanxi University, Taiyuan, Shanxi 030006, People's Republic of China*

³*Department of Physics and Astronomy, Shanghai Jiao Tong University, Shanghai 200240, China*

(Received 22 November 2016; published 21 June 2017)

We experimentally demonstrate two types of peak-peak delay effects in linear and high-gain saturation regions of a stimulated Raman process in ⁸⁷Rb atomic vapor. The delay time linearly increases with the intensity of the Raman pump field in the linear Raman amplifier due to the slow-light effect but is independent of the intensity of the input weak seed pulse. In contrast, in a high-gain saturation region, the delay time decreases with the intensities of not only the Raman pump but also the input seed fields because of the large Raman coupling coefficient and serious depletion of the atoms. In particular, when the input seed contains several photons per pulse on average, the peak-peak delay time linearly decreases with the number of photons in the input seed pulse, showing that the Stokes seed at the few-photon level still has a significant effect on the peak-peak delay.

DOI: 10.1103/PhysRevA.95.063834

I. INTRODUCTION

The optical pulse time-delay effect has been observed using resonant techniques, such as electromagnetically induced transparency (EIT) [1], in atomic vapors [2,3] and solids [4,5]. However, the time delay of optical signals using the EIT technique is limited by the long pulse and non-negligible loss in practical applications. Moreover, there are many nonlinear optical techniques based on nonresonant interactions [6,7]. Stimulated Raman scattering (SRS) [8,9], one nonresonant interaction, has also been demonstrated to produce pulse-peak delay at several nanoseconds and picoseconds in solid [10–13] and liquid [14] systems. The mechanism for such a time-delay effect has been theoretically analyzed based on optically induced slow-light effects on a weak pulse [15]. Compared with EIT, the time-delay effect in stimulated Raman scattering is more practical because of the shorter pulse width of the optical pulse and lower intensity loss. However, the delay times in the above processes, including EIT and SRS, are not related to the intensities of the input weak optical pulses.

Atomic vapors are good systems for precision measurement and optical communication. In this paper, we experimentally demonstrate two types of peak-peak delay effects in ⁸⁷Rb atomic vapor via a stimulated Raman process. In the linear Raman amplifier region, we find that the delay time increases with the intensity of a strong Raman pump pulse, which is caused by the slow light mechanism, as predicted by linear theory [15,16], and can be useful for optical communication. In the high-gain saturation regime [8,15], a different peak-peak delay effect appears in the stimulated Raman process. The peak-peak delay time decreases with the intensities of not only the Raman pump field but also the Stokes seed pulses simultaneously mainly due to the large Raman coupling coefficient and significant dissipation of atoms. In such high-gain saturation regimes, when the power of the input seed

pulse decreases until it contains only a few photons in each pulse, the peak-peak delay also depends on the intensity of the Stokes seed pulse and is inversely proportional to the photon number of the input seed pulse.

Our article is organized as follows. In Sec. II, we theoretically describe the group velocity and the delay time of the Stokes field. The experimental setup is given in Sec. III. In Sec. IV, we demonstrate the experimental results and give the theoretical analysis. Finally, we conclude with a summary of our results.

II. GROUP VELOCITY AND DELAY TIME

In this section, we will briefly review the model for the stimulated Raman scattering process [8,17] with energy level configuration shown in Fig. 1, and present the group velocity and the delay time of the Stokes field.

In the dipole and rotating wave approximations, the Hamiltonian is given by [8,17]

$$H = H_{\text{atoms}} + H_I, \quad (1)$$

where

$$H_{\text{atoms}} = \hbar\omega_{eg}|e\rangle\langle e| + \hbar\omega_{mg}|m\rangle\langle m|, \quad (2)$$

$$H_I = -\hbar(\Omega_P e^{i(k_P z - \omega_P t)}|e\rangle\langle g| + \Omega_S e^{i(k_S z - \omega_S t)}|e\rangle\langle m|) + \text{H.c.} \quad (3)$$

Here $\omega_{eg} = \omega_e - \omega_g$ and $\omega_{mg} = \omega_m - \omega_g$. $2\Omega_P = \mu_{eg}\mathcal{E}_P/\hbar$ and $2\Omega_S = \mu_{em}\mathcal{E}_S/\hbar$ are the Rabi frequencies associated with the coupling of the field modes of frequencies ω_P and ω_S to the atomic transitions $|e\rangle \rightarrow |g\rangle$ and $|e\rangle \rightarrow |m\rangle$, respectively. The two optical fields are described in terms of their slowly varying amplitudes $\mathcal{E}_P(z,t)$ and $\mathcal{E}_S(z,t)$.

*lqchen@phy.ecnu.edu.cn

†chyuan@phy.ecnu.edu.cn

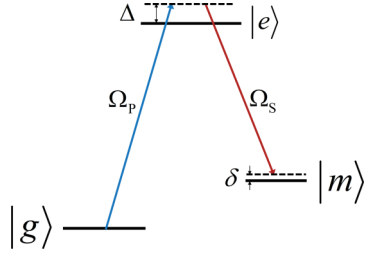


FIG. 1. Schematic diagram of three-level atoms. Ω_P, Ω_S : the Rabi frequencies of Raman pump field and Stokes field, respectively; Δ, δ : the detunings.

The density matrix equations of motion are given by

$$\begin{aligned} \frac{d}{dt} \tilde{\rho}_{gg} &= \Gamma_{eg} \tilde{\rho}_{ee} + i\Omega_P^* \tilde{\rho}_{eg} - i\Omega_P \tilde{\rho}_{ge}, \\ \frac{d}{dt} \tilde{\rho}_{mm} &= \Gamma_{em} \tilde{\rho}_{ee} + i\Omega_S^* \tilde{\rho}_{em} - i\Omega_S \tilde{\rho}_{em}, \\ \frac{d}{dt} \tilde{\rho}_{gm} &= -(\gamma_{gm} + i\delta) \tilde{\rho}_{gm} + i\Omega_P^* \tilde{\rho}_{em} - i\Omega_S \tilde{\rho}_{ge}, \\ \frac{d}{dt} \tilde{\rho}_{ge} &= -(\gamma_{ge} + i\Delta) \tilde{\rho}_{ge} + i\Omega_P^* n_{eg} - i\Omega_S^* \tilde{\rho}_{gm}, \\ \frac{d}{dt} \tilde{\rho}_{em} &= -[\gamma_{em} - i(\Delta - \delta)] \tilde{\rho}_{em} + i\Omega_P \tilde{\rho}_{gm} - i\Omega_S n_{em}, \end{aligned} \quad (4)$$

where the detunings $\Delta = \omega_P - \omega_{eg}$ and $\delta = \omega_P - \omega_S - \omega_{mg}$; the density matrix substitutions $\rho_{gm} = \tilde{\rho}_{gm} e^{i(\omega_P - \omega_S)t - i(k_P - k_S)z}$, $\rho_{ge} = \tilde{\rho}_{ge} e^{i(\omega_P t - k_P z)}$, and $\rho_{em} = \tilde{\rho}_{em} e^{-i(\omega_P t - k_P z)}$; and where $\tilde{\rho}_{kl}$ are slowly varying in time and space. Γ_{eg} and Γ_{em} are the radiative decay terms from the excited state $|e\rangle$ to the two ground states $|g\rangle$ and $|m\rangle$, respectively. γ_{kl} is the nonradiative decoherence of $\tilde{\rho}_{kl}$ ($k \neq l$). $n_{kl} = \tilde{\rho}_{kk} - \tilde{\rho}_{ll}$ is the atomic population difference between the states $|k\rangle$ and $|l\rangle$. Now we are in a position to solve for properties of the system. The steady-state density matrix element $\tilde{\rho}_{em}$ is given by

$$\tilde{\rho}_{em} = -i \frac{\Omega_S \frac{|\Omega_P|^2}{\gamma'_{ge}} n_{ge} + \left(\gamma'_{gm} + \frac{|\Omega_S|^2}{\gamma'_{ge}} \right) n_{em}}{\gamma'_{em} \frac{|\Omega_P|^2}{\gamma'_{em}} + \left(\gamma'_{gm} + \frac{|\Omega_S|^2}{\gamma'_{ge}} \right)}, \quad (5)$$

where $\gamma'_{gm} = \gamma_{gm} + i\delta$, $\gamma'_{ge} = \gamma_{ge} + i\Delta$ and $\gamma'_{em} = \gamma_{em} - i(\Delta - \delta)$. Due to the large one-photon detuning Δ , small two-photon detuning δ , and $|\Omega_S| \ll |\Omega_P|$ in the Raman scattering, the above equation can be reduced to

$$\tilde{\rho}_{em} \approx \frac{\Omega_S \gamma_{gm} n_{em} + \frac{|\Omega_P|^2}{\Delta^2} \gamma_{ge} n_{ge} - i(\delta_L + \delta) n_{ge}}{\Delta \gamma_{gm} + \frac{|\Omega_P|^2}{\Delta^2} \gamma_{em} + i(\delta_L + \delta)}, \quad (6)$$

where $\delta_L = |\Omega_P|^2/\Delta$ is the ac Stark shift. A suitable two-photon detuning δ can compensate this Stark frequency shift δ_L to make $(\delta_L + \delta) \sim 0$. But if $\delta \sim 0$ and the pump field is so strong that δ_L is large enough as compared to γ_{gm} , the Stark shift will be significant in slow-light effects.

Then from Eq. (6), we can evaluate the linear and nonlinear components of the polarization at ω_S [18]

$$P = \tilde{P}(\omega_S) e^{-i\omega_S t} + \text{c.c.}, \quad (7)$$

where $\tilde{P}(\omega_S) = (N/V) \mu_{me} \tilde{\rho}_{em}$ is described by the average dipole moment of the atoms. N is the atom number in the light-atom interaction region and V is the volume of the interaction region. The Raman susceptibility $\chi_R(\omega_S = \omega_S + \omega_P - \omega_P)$ can be given from the expression

$$\tilde{P}(\omega_S) = 6\epsilon_0 \chi_R |\mathcal{E}_P|^2 \mathcal{E}_S. \quad (8)$$

Finally, the light group velocity is $v_g = c/[n + \omega(dn/d\omega)]_{\omega=\omega_S}$ [11] with $n \simeq 1 + \text{Re}[\chi_R]/2$, and the delay time between input and output Stokes pulses is approximately given by

$$\begin{aligned} \tau &= L \left(\frac{1}{v_g} - \frac{1}{c} \right) \\ &= \frac{L}{2c} \left\{ \text{Re}[\chi_R] + \omega \text{Re} \left[\frac{d\chi_R}{d\omega} \right] \right\}_{\omega=\omega_S}. \end{aligned} \quad (9)$$

In the present paper, we will consider two special cases: linear and high-gain Raman scatterings. In most research on the slow-light effect in linear Raman scattering such as in Refs. [10–13], the Raman gain is small and only a small proportion of atoms is moved to the $|m\rangle$ level, i.e., $\tilde{\rho}_{gg} \approx 1$. In such linear Raman scattering, the Stark shift δ_L can be negligible because $|\Omega_P|^2/\Delta \ll \gamma_{gm}$. With $\delta \sim 0$ and $\mu_{kl} = \mu_{lk}$, the density matrix element $\tilde{\rho}_{em}$ is

$$\tilde{\rho}_{em} \simeq -\frac{|\Omega_P|^2 \Omega_S}{\Delta^3 \gamma_{gm}^2} (|\Omega_P|^2 + i\Delta \gamma_{gm}), \quad (10)$$

and the Raman susceptibility χ_R is given by

$$\chi_R = -\frac{N \mu_{me}^2 |\mu_{eg}|^2}{48\epsilon_0 V \hbar^3 \Delta^3 \gamma_{gm}^2} [|\Omega_P|^2 + i\Delta \gamma_{gm}]. \quad (11)$$

According to Eq. (9), the delay time is

$$\begin{aligned} \tau_L &= -\frac{L}{2c} \frac{N \mu_{me}^2 |\mu_{eg}|^2 |\Omega_P|^2}{48\epsilon_0 V \hbar^3 \Delta^3 \gamma_{gm}^2} \left(1 - \frac{3\omega_S}{\Delta} \right) \\ &\simeq \frac{LN \mu_{me}^2 |\mu_{eg}|^4 \omega_S |\mathcal{E}_P|^2}{128\epsilon_0 V \hbar^5 \gamma_{gm}^2 c \Delta^4}, \end{aligned} \quad (12)$$

where subscript L denotes the linear region.

On the other hand, in high-gain Raman scattering, the Raman coupling coefficient is very large, i.e., $\delta_L = |\Omega_P|^2/\Delta \gg \gamma_{gm}$, and many atoms can be driven to the $|m\rangle$ level, even leading to $n_{gm} < 0$. With $\delta_L \gg \gamma_{gm}$ and $\delta \sim 0$, the density matrix element $\tilde{\rho}_{em}$ can be written as

$$\tilde{\rho}_{em} \simeq -\frac{\Omega_S}{\Delta} \tilde{\rho}_{gg} - i\Omega_S \left[\left(\frac{\gamma_{gm}}{|\Omega_P|^2} + \frac{\gamma_{ge}}{2\Delta^2} \right) n_{gm} + \frac{\gamma_{ge}}{2\Delta^2} \right], \quad (13)$$

and the corresponding Raman susceptibility is

$$\begin{aligned} \chi_R &= -\frac{N \mu_{me}^2}{12\hbar \epsilon_0 V |\mathcal{E}_P|^2} \left[\frac{1}{\Delta} \tilde{\rho}_{gg} + i \frac{\gamma_{ge}}{2\Delta^2} \right. \\ &\quad \left. + i \left(\frac{\gamma_{gm}}{|\Omega_P|^2} + \frac{\gamma_{ge}}{2\Delta^2} \right) n_{gm} \right]. \end{aligned} \quad (14)$$

In the high-gain region, the delay time is given by

$$\begin{aligned} \tau_H &= -\frac{LN\mu_{me}^2\tilde{\rho}_{gg}}{24c\hbar\epsilon_0V|\mathcal{E}_P|^2\Delta}\left(1-\frac{\omega_S}{\Delta}\right) \\ &\simeq \frac{LN\mu_{me}^2\omega_S n_{gm} + 1}{48c\hbar\epsilon_0V|\mathcal{E}_P|^2\Delta^2}, \end{aligned} \quad (15)$$

where subscript H denotes the high-gain region. The above equation describes the relation of delay time τ with the detuning Δ , amplitude \mathcal{E}_P of the pump field, and the population difference n_{gm} .

To describe the propagation of light through the medium, the wave equation is used and given as follows:

$$\nabla^2\mathbf{E} - \frac{1}{c^2}\frac{\partial^2\mathbf{E}}{\partial t^2} = \frac{1}{\epsilon_0c^2}\frac{\partial^2\mathbf{P}}{\partial t^2}, \quad (16)$$

where \mathbf{P} is the polarization induced in the atomic ensemble. In a stimulated Raman scattering process with an input Stokes seed of single transverse spatial mode, the above equation can be simplified to a one-dimensional model. Under the condition of a slowly varying amplitude approximation, the wave equation for Stokes field \mathcal{E}_S is given by

$$\frac{\partial}{\partial z}\mathcal{E}_S + \frac{1}{c}\frac{\partial}{\partial t}\mathcal{E}_S = \frac{ik_S}{2\epsilon_0V}\mu_{me}\tilde{\rho}_{em}. \quad (17)$$

By eliminating the atomic degrees of freedom, we get an effective equation for the field only, involving the susceptibilities, to analyze the propagation of light through the atomic ensemble. In the linear and high-gain regions, we have the respective optical Bloch equations for Stokes fields \mathcal{E}_S :

$$\frac{\partial}{\partial z}\mathcal{E}_S + \frac{1}{c}\frac{\partial}{\partial t}\mathcal{E}_S = g_L\left(1 - i\frac{|\Omega_P|^2}{\Delta\gamma_{gm}}\right)\mathcal{E}_S, \quad (18)$$

$$\frac{\partial}{\partial z}\mathcal{E}_S + \frac{1}{c}\frac{\partial}{\partial t}\mathcal{E}_S = g_H\mathcal{E}_S - i\frac{Nk_S\mu_{em}^2\sqrt{\tilde{\rho}_{gg}}}{4\hbar\epsilon_0V\Delta}\mathcal{E}_S, \quad (19)$$

where

$$g_L = \frac{Nk_S\mu_{em}^2|\Omega_P|^2}{4\hbar\epsilon_0V\Delta^2\gamma_{gm}}, \quad (20)$$

$$g_H = \frac{Nk_S\mu_{em}^2}{4\hbar\epsilon_0V}\left[\left(\frac{\gamma_{gm}}{|\Omega_P|^2} + \frac{\gamma_{ge}}{2\Delta^2}\right)n_{gm} + \frac{\gamma_{ge}}{2\Delta^2}\right]. \quad (21)$$

The imaginary component of Raman susceptibility is related to the Raman gain profile. In the linear region, the Raman gain is $G_L = e^{2g_L z} \simeq 1 + 2g_L z$, and $G_H = e^{2g_H z}$ is the Raman gain in the high-gain region. The intensity of the amplified Stokes field can be written as $I_S = G_j I_S^{(im)}$ ($j = L, H$).

III. EXPERIMENTAL SETUP

The experimental sketch is shown in Fig. 2(a), where the stimulated Raman process is operated in a hot ^{87}Rb atomic vapor. The ^{87}Rb atoms are contained in a 50-mm-long paraffin-coated glass cell, which is placed inside a four-layer μ -magnetic shielding to reduce stray magnetic fields and is heated to 72°C using a resistive heater. The energy levels of ^{87}Rb atoms with relevant detunings and time sequence are shown in Figs. 2(b) and 2(c), respectively. The lower two energy states $|g\rangle$ and $|m\rangle$ are the hyperfine-split

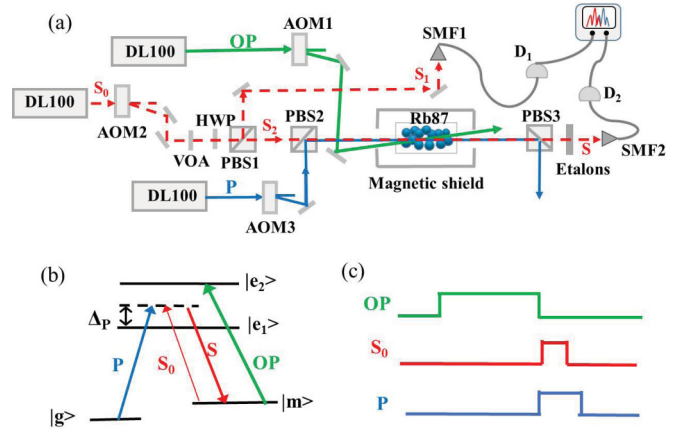


FIG. 2. (a) Experimental setup. AOM: acousto-optic modulator; VOA: variable optical attenuator; SMF: single-mode fiber; PBS: polarization beam splitter; HWP: half-wave plate. OP: optical pumping pulse; P: Raman pump pulse; S_0 : input Stokes pulse; and S: generated Stokes signal. (b) Energy levels with relevant detunings for stimulated Raman scattering. $|g\rangle$: $|5^2S_{1/2}, F = 1\rangle$; $|m\rangle$: $|5^2S_{1/2}, F = 2\rangle$. The two higher energy states $|e_1\rangle$ and $|e_2\rangle$ are the excited states $|5^2P_{1/2}, F = 2\rangle$ and $|5^2P_{3/2}, F = 3\rangle$, respectively. Δ_P : detuning frequency of Raman pump field. (c) Time sequence.

ground states $|5^2S_{1/2}, F = 1, 2\rangle$ with a frequency difference of 6.83 GHz. The two higher energy states $|e_1\rangle$ and $|e_2\rangle$ are the excited states $|5^2P_{1/2}, F = 2\rangle$ and $|5^2P_{3/2}, F = 3\rangle$, respectively. Approximately 98% of the atoms are initially prepared in the ground state $|g\rangle$ by a $40\ \mu\text{s}$ -long OP pulse. The optical pumping laser (OP) resonates on $|m\rangle \rightarrow |e_2\rangle$. After the OP pulse, we turn on the Raman pump pulse (P) and input the Stokes seed pulse (S_0). The S_0 pulse is 50 ns long, and the P pulse is $5\ \mu\text{s}$. The P laser is detuned from the $|g\rangle \rightarrow |e_1\rangle$ transition by $\Delta_P = 0.2\text{--}1.5$ GHz. The S_0 field comes from another semiconductor laser, whose frequency is locked on the P laser by a 6.83-GHz frequency difference using a phase-locked loop. Before entering the cell, the S_0 pulse is separated into two, S_1 and S_2 , by a polarizing beam splitter (PBS1) and a half-wave plate (HWP). The intensities of the S_1 and S_2 fields are made the same by rotating the HWP. The S_1 field is coupled into a single-mode fiber and is detected by detection system D_1 directly to act as the intensity and time references for S_2 . The S_2 pulse as the Raman seed is sent into the cell spatially overlapping with the P field to generate the output field (S) via the stimulated Raman process. The waists of the OP, P, and S_2 fields at the center of the cell are 1.2, 0.6, and 0.6 mm, respectively. We use two filters to separate the output S photons from the P photons. The first filter is the PBS3 to filter out most of the P photons with a 30-dB extinction ratio. The second filter is the optical etalons. An etalon can filter out the leaked P photons at 29 dB, with a transmission of the S photons at 80%. Finally, the output S field is coupled into a single-mode fiber and detected by the detection system D_2 .

IV. EXPERIMENTAL RESULTS AND DISCUSSION

A. Slow-light-induced time-delay effect

First, we investigate the time-delay effect in atomic vapor in linear stimulated Raman scattering, in which the Raman gain

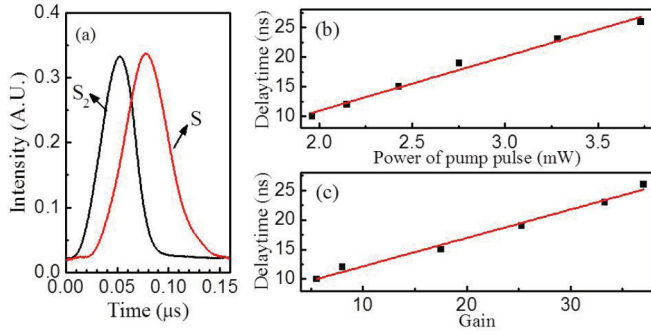


FIG. 3. Peak delay effect in the linear Raman amplifier. (a) Temporal shapes of the S_2 and S pulses. Black curve: S_2 pulse; red curve: amplified output Stokes S pulse. The powers of the seed and Raman pump fields S_2 are $1.0 \mu\text{W}$ and 3.3 mW . $\Delta_P = 1.5 \text{ GHz}$. The power of the S field is normalized to the S_2 field. The delay times as a function of (b) the powers of the Raman pump pulses and (c) the Raman gain. The squares represent experimental results, and the red solid curve is the linear fit.

(dividing the energy of the S pulse by that of the input seed pulse) is low and linearly depends on the power of the Raman pump field but has no relation to the power of the input seed pulse. The temporal profiles of the input seed S_2 and amplified Stokes S pulses are given in Fig. 3(a) with a Raman gain factor of 32. The input seed S_2 and amplified S fields are sufficiently strong to be recorded directly using a photodetector and an oscilloscope. The peak-peak time delay between the S_2 and S pulses is clearly observed. In the meantime, a slight broadening of the input pulse is also observed, which is caused by the bandpass filtering effect because of the limited bandwidth of stimulated Raman scattering. The delay time τ as a function of the power of the Raman pump pulse and Raman gain are given in Figs. 3(b) and 3(c), respectively. The delay time τ increases linearly with the intensity of the pump pulse and the Raman gain. The slopes are approximately 4 ns/mW and 0.5 ns/time .

From Eqs. (12) and (20), the peak-peak time delay between the S_2 and S pulses is linearly proportional to the intensity of the Raman pump field and the Raman gain, which is given by

$$\tau_L \propto |\mathcal{E}_P|^2 \propto g_L/\Delta^2 \propto (G_L - 1)/\Delta^2. \quad (22)$$

In our experiment, the number of atoms in the pump beam is $\sim 2.5 \times 10^9$, and the photon number in the S pulse in Fig. 3(a), which is roughly equal to the number of atoms on the $|m\rangle$ level, is about 1.0×10^7 , then $n_{gm} = 0.99 \sim 1$. Our experimental results of the peak-peak delay effect in Fig. 3 agree with our theoretical prediction.

Such a time-delay effect is due to the optically induced slow-light effect on a weak pulse in an off-resonant Raman medium, which was also demonstrated in solid and liquid systems with much stronger pump intensity [10–12, 14]. But in a ^{87}Rb atomic vapor, the delay time is larger than that in solid systems. This type of slow-light-induced pulse delay effect in atomic vapor can be very useful for optical communication.

B. Photon-number-dependent time-delay effect

Next, we demonstrate the pulse-peak delay effect via stimulated Raman scattering in the high-gain regime [8], which

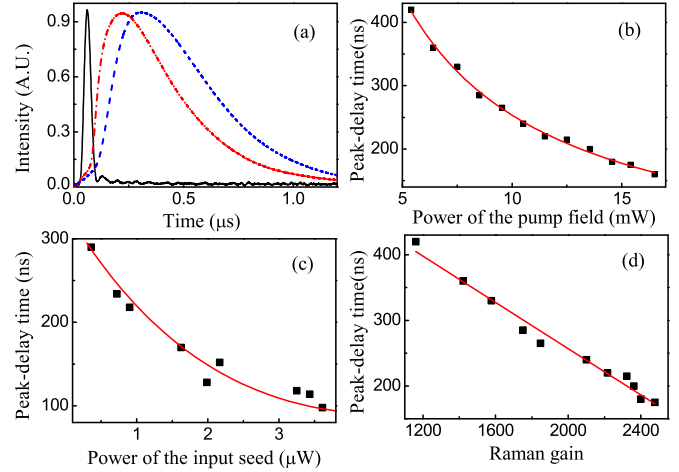


FIG. 4. Peak delay effect in the stimulated Raman scattering in the high-gain regime. (a) The temporal shapes of the S_2 and S pulses. $\Delta_P = 400 \text{ MHz}$. Black curve: S_2 pulse; red dash-dot curve: S pulse with the 15.8-mW Raman pump and a Raman gain of 1200; blue dashed curve: S pulse with the 9.2-mW Raman pump and a Raman gain of 850. The power of the seed field S_2 is $1.2 \mu\text{W}$. The power of the S field is normalized to the S_2 field. The delay time as a function of (b) the power of the Raman pump field and (c) the input S_2 pulse. The squares represent experimental results, and the red curve is the fit using reciprocal function in (b) and function of $a + bx e^{-cx}$ in (c). The power of the input seed field is $1.2 \mu\text{W}$ and $\Delta_P = 400 \text{ MHz}$ in (b). The power of the Raman pump field is 15.5 mW and $\Delta_P = 350 \text{ MHz}$ in (c). (d) Peak-delay time as a function of the Raman gain.

is also the key point of this paper. Compared with solid systems, the high-gain stimulated Raman scattering can be achieved easily in atomic vapor by adjusting the frequency and power of the pump field in experiment because of the long atomic coherence time.

Figure 4(a) shows the temporal behaviors of the Stokes field S_1 (the reference of S_2) and S with Raman gains of 850 (blue dashed line) and 1200 (red dash-dot line). The corresponding photon numbers in the S pulses are approximately 0.5×10^9 ($n_{gm} = 0.6$) and 0.72×10^9 ($n_{gm} = 0.42$) and the Stark shifts are about 37 and 64 MHz, respectively. The peak-peak delay is also observed. To obtain greater insight into the dependence between the peak-peak delay and the experimental parameters, several delay times were measured and are given as a function of the power of the Raman pump in Fig. 4(b) and input seed in Fig. 4(c). In contrast to the linear Raman amplifier in Fig. 3, both curves show decay dependence, indicating that the delay times between the peaks of the input and output Stokes pulses in the high-gain Raman amplifier decrease with the powers of not only the pump but also the seed fields. In addition, the peak-peak delay time decreases with the Raman gain in Fig. 4(d). These different dependencies are mainly caused by the large Raman coupling coefficient and the significant depletion of the atoms on the $|g\rangle$ state represented by the population difference n_{gm} in the high-gain Raman process as our theory predicted.

In the high-gain stimulated Raman scattering process, the number of Stokes light is approximately equal to the number of atomic excitation, then $n_{gm} \approx 1 - 2G_H N_{S_0}/N$ where N_{S_0} is the photon number of the input seed pulse and G_H is Raman

gain. From Eq. (15), the delay time is

$$\tau_H \propto \frac{n_{gm} + 1}{|\mathcal{E}_P|^2} \propto \frac{1 - G_H N_{S_0}/N}{I_P}. \quad (23)$$

The delay time τ_H is inversely proportional to the intensity of the pump field and decreases with Raman gain G_H , which matches well with the experimental results in Figs. 4(b) and 4(d). Furthermore, by only changing the photon number of the input seed pulse, the gain G_H can be written as

$$G_H \propto \exp(c_1 - c_2 N_{S_0}), \quad (24)$$

where c_1 and c_2 are coefficients. When N_{S_0} is small compared with the atom number N , the delay time τ_H near-linearly decreases with the photon number of the input Stokes seed N_{S_0} . However, when N_{S_0} increases, G_H will exponentially decrease, which leads to a slower decline of τ_H as shown Fig. 4(c). The experimental results qualitatively match the theoretical predictions well.

In addition, the decoherence rate γ_{gm} of the atomic system is neglected in Eq. (15). The atomic coherence time is an important parameter for achieving high-gain Raman scattering. In an atomic vapor without a buffer gas, the coherence time is mainly limited by the coherent atoms flying out of the region of the pump beam, which is $\sim 1.2 \mu\text{s}$ in our experiment as shown in Fig. 5, and much larger than that in solid systems [11,12,14,15]. In Fig. 4, the peak delay time is smaller than $0.5 \mu\text{s}$, which is much shorter than the coherence time $1.2 \mu\text{s}$. In such short delay time, only a small number of coherent atoms fly out of the pump beam region, so decoherence has a small effect on the intensity of the amplified Stokes and delay time.

The population difference n_{gm} in Eq. (15) only relates with the coherent transition by stimulated Raman scattering (the photon number in the S pulse). But in a real experiment of atomic vapor, n_{gm} depends on not only coherent transition by stimulated Raman scattering but also incoherent exchange of the atoms between the interaction and non-interaction regions.

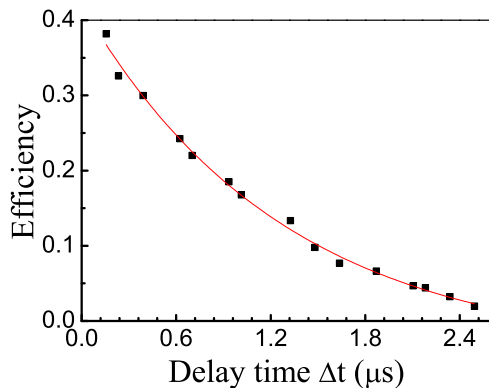


FIG. 5. Retrieve efficiency as a function of delay time. A read pulse is turned on to readout the atomic spin wave in the atomic ensemble. The read pulse detunes 1.5 GHz from the $|m\rangle \rightarrow |e_1\rangle$ transition and lasts 200 ns. The power of the read field is 50 mW. The delay time Δt is measured from the end of the Raman pump pulse and the beginning of the read pulse. The squares represent the experimental data and the red line is the exponential decay fitting curve. The fitting coherent time is about $1.2 \mu\text{s}$.

The $|m\rangle$ atoms outside the optical pump beam will fly into the interaction region, and the $|g\rangle$ atoms in the interaction region will fly out of the Raman pump beam. Incoherent exchange depends on atomic speed with 400 m/s in atomic vapor. In Fig. 4 with $\tau < 0.5 \mu\text{s}$, a small number of atoms on the $|m\rangle$ level outside the optical pump beam with the diameter of 1.2 mm fly into the interaction region with the diameter of 0.6 mm. Therefore, in the case of such a short delay time, the incoherent exchange effect on n_{gm} can be neglected. Reduction of the population difference n_{gm} is mainly caused by coherent transition.

Finally, we reduce the power of the input seed to several photons per pulse on average using a variable optical attenuator. When the S_1 (the reference of S_2) pulse only contains several photons, the photon number is recorded by a single-photon detector and a counter. Its temporal behavior is measured using the single-photon detection system consisting of a single-photon detector, a time-to-amplitude converter, and a multichannel pulse amplitude analyzer (MPA). The time resolution of the MPA is approximately 1.0 ns. In Fig. 6(a), the input seed S_2 pulse contains 3.0 photons per pulse on average, corresponding to the power of 0.6×10^{-12} W. The S pulse is amplified 1.1×10^4 times to 0.66×10^{-8} W. In the experiment, the power of the P pulse is tens of milliwatts, which is reduced to $\sim 10^{-5}$ W after PBS3 and then to $10^{-10} \sim 10^{-11}$ W after two etalons. So the leaked P photons can be neglected compared with the S pulses [0.66×10^{-8} W, $\sim 1 \times 10^5$ photons in the S pulse in Fig. 6(a)]. The intensity of the S pulse after two etalons is about 1×10^{-9} W, which is too weak to be detected with a photodiode detector directly but too strong to be detected with a single-photon detector directly. Therefore, in the experiment a 30-dB optical attenuator is placed between the etalons and the SMF2 to reduce the S pulse to 1×10^{-12} W (approximate two photons per 50 ns) before the single-photon detector. The temporal shape of the S pulse is measured by recording 10^5 shots using the single-photon detection system.

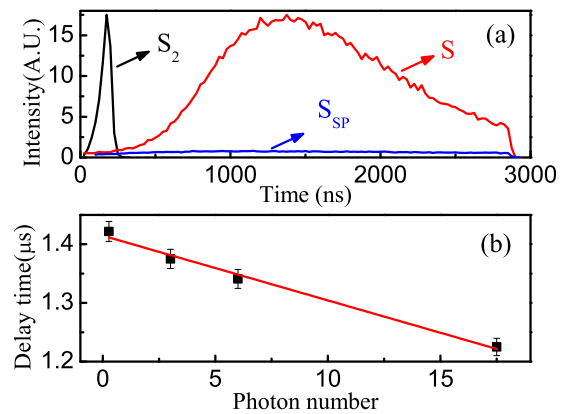


FIG. 6. (a) Temporal shapes of the S_2 and S pulses. Black curve: S_2 field containing 3.0 photons on average per pulse; red curve: S field with the S_2 field entering the atomic vapor; blue curve: S_{SP} , with the S field obtained by blocking the S_2 field before the cell. The power of the S_2 field is normalized to the S field. (b) Delay time as a function of the number of photons in each S_2 pulse on average. $\Delta_p = 300$ MHz. The power of the Raman pump field is 4.0 mW.

The intensity-normalized results are shown in Fig. 6(a). Note that the width of the S pulse is much longer than that of the S_2 pulse, and the amplified S pulse consists of two parts: one part arising from the spontaneous Raman scattering (S_{Sp}) and the other part amplified from the input seed by stimulated Raman scattering (S_{St}). The S_{Sp} curve is measured by blocking the S_2 field before entering the cell. The intensity of the S_{Sp} field is approximately 1/10 of that of the S pulse, indicating that S_{St} is the main component of the S pulse. The important parameter of concern in Fig. 6(a), the delay time between the pulse peaks of S_2 and S, is prolonged to $1.37 \mu\text{s}$, and the temporal width of the S pulse is longer than the atomic decoherence time ($\sim 1.2 \mu\text{s}$). In such a long delay time, most atomic spin waves fly out of the interaction region, which will limit the amplification of the S pulse beyond the coherent time. And many $|m\rangle$ atoms outside the pump beam also fly into the interaction region. Thus, the population difference n_{gm} in Eq. (15) is determined by not only the coherent transition effect related to the intensities of the pump and input seed fields but also the incoherent exchange factor. To investigate the peak-peak delay effect with input seed pulses containing several photons per pulse, we measure the delay time with different photon numbers in the seed pulse. The results are given in Fig. 6(b). The delay time is near-inversely proportional to the photon number due to exponential decay near its decay origin as shown in Eq. (15). The slope of the linear fit is approximately 11.0 ns/photon. These results show that even at the few-photon level the Stokes seed also has a significant

effect on the peak-peak delay in high-gain Raman scattering processes.

V. CONCLUSIONS

We have demonstrated the peak-peak delay effect between the input seed pulse and the amplified Stokes signal in a stimulated Raman process in ^{87}Rb atomic vapor. The delay time is proportional to the intensity of the Raman pump field in the linear Raman amplifier. In high-gain Raman scattering, the delay time is the tendency to decay along with the intensities of the Raman pump and input seed fields simultaneously. In particular, even at the few-photon level, the Stokes seed still has significant effect on the peak-peak delay, which is near-linearly related to the photon number of the input seed pulse. In Raman processes, it is possible not only to control the group velocity of the weak light and but also to amplify it coherently. It may have potential applications in optical buffers and repeaters.

ACKNOWLEDGMENTS

This work is supported by the National Key Research and Development Program of China under Grant No. 2016YFA0302001, the National Natural Science Foundation of China (Grants No. 91536114, No. 11474095, and No. 11234003), and Natural Science Foundation of Shanghai (Grant No. 17ZR1442800).

-
- [1] M. Fleischhauer, A. Imamoglu, and J. P. Marangos, *Rev. Mod. Phys.* **77**, 633 (2005).
 - [2] M. Mücke, E. Figueroa, J. Bochmann, C. Hahn, K. Murr, S. Ritter, C. J. Villas-Boas, and G. Rempe, *Nature* **465**, 755 (2010).
 - [3] A. V. Gorshkov, A. André, M. Fleischhauer, A. S. Sørensen, and M. D. Lukin, *Phys. Rev. Lett.* **98**, 123601 (2007).
 - [4] J. J. Longdell, E. Fraval, M. J. Sellars, and N. B. Manson, *Phys. Rev. Lett.* **95**, 063601 (2005).
 - [5] A. H. Safavi-Naeini, T. P. Mayer Alegre, J. Chan, M. Eichenfield, M. Winger, Q. Lin, J. T. Hill, D. E. Chang, and O. Painter, *Nature* **472**, 69 (2011).
 - [6] J. E. Sharping, Y. Okawachi, and A. L. Gaeta, *Opt. Express* **13**, 6092 (2005).
 - [7] Z. Zhu, D. J. Gauthier, Y. Okawachi, J. E. Sharping, A. L. Gaeta, R. W. Boyd, and A. E. Willner, *J. Opt. Soc. Am. B* **22**, 2378 (2005).
 - [8] M. G. Raymer and J. Mostowski, *Phys. Rev. A* **24**, 1980 (1981).
 - [9] F. Benabid, J. C. Knight, G. Antonopoulos, and P. S. J. Russell, *Science* **298**, 399 (2002).
 - [10] J. Q. Liang, M. Katsuragawa, F. L. Kien, and K. Hakuta, *Phys. Rev. A* **65**, 031801(R) (2002).
 - [11] K. Lee and N. M. Lawandy, *Appl. Phys. Lett.* **78**, 703 (2001).
 - [12] G. Qin, R. Jose, and Y. Ohishi, *J. Appl. Phys.* **101**, 093109 (2007).
 - [13] O. D. Herrera, L. Schneebeli, K. Kieu, R. A. Norwood, and N. Peyghambarian, *Opt. Express* **21**, 8821 (2013).
 - [14] P. Chýlek, A. Biswas, M. A. Jarzembki, V. Srivastava, and R. G. Pinnick, *Appl. Phys. Lett.* **52**, 1642 (1988).
 - [15] F. L. Kien and K. Hakuta, *Can. J. Phys.* **78**, 543 (2000).
 - [16] M. G. Payne and L. Deng, *Phys. Rev. A* **64**, 031802(R) (2001).
 - [17] C.-H. Yuan, L. Q. Chen, J. T. Jing, Z. Y. Ou, and W. Zhang, *Phys. Rev. A* **82**, 013817 (2010).
 - [18] R. W. Boyd, *Nonlinear Optics* (Academic, New York, 1992).